SEARCH FOR PNC IN ATOMIC DYSPROSIUM

A.-T. NGUYEN,* D.E. BROWN,* D. BUDKER,*† D. DEMILLE,*‡
D.F. KIMBALL,* and M. ZOLOTOREV§
*Physics Department, University of California, Berkeley,
CA 94720-7300, USA
e-mail: budker@socrates.berkeley.edu

†Nuclear Science Division, E. O. Lawrence Berkeley National Laboratory, Berkeley,
CA 94720, USA

‡Present address: Department of Physics, Yale University, New Haven,
CT 06520, USA

§Center for Beam Physics, E. O. Lawrence Berkeley National Laboratory, Berkeley,
CA 94720, USA

Results and current progress of a search for parity nonconservation (PNC) in a pair of nearly degenerate opposite parity states in atomic dysprosium are discussed. By observing time-resolved quantum beats between these sublevels, we look for interference between a Stark-induced amplitude and the much smaller PNC amplitude. We have reported elsewhere (A.-T. Nguyen, et. al., *Phys. Rev.* A **56**, 3453 (1997)) a value of $|H_w| = |2.3 \pm 2.9(statistical) \pm .7(systematic)|$ Hz for the magnitude of the weak interaction matrix element. In order to increase the statistical sensitivity in a new search, we will employ a cw scheme for excitation and detection. This involves utilizing cw lasers to populate the odd parity level via two intermediate states. We have measured various spectroscopic parameters of the intermediate states including branching ratios, lifetimes, isotope shifts, and hyperfine structure. Furthermore, we have modeled an efficient scheme for coherent population transfer using diverging cw Gaussian laser beams and adiabatic passage. This should increase statistical sensitivity to PNC effects by several orders of magnitude.

1 Introduction

Dysprosium (Z=66) is of interest for PNC experiments because of a near degeneracy of a pair of opposite parity levels (see Fig. 1) which serves to enhance the level mixing caused by the weak interaction. This small energy level separation is on the order of hyperfine splittings and isotope shift energies, and enables one to use techniques quite different than those used in traditional PNC experiments. In addition, the existence of many stable isotopes in dysprosium allows for a determination of the weak charge through isotopic comparisons, eliminating the uncertainties associated with atomic calculations. [1] Finally, measurements of nuclear anapole moments are possible with ^{161}Dy and ^{163}Dy, both with nuclear spin $I = 5/2$. The anapole moments manifest

themselves as the dependence of PNC on nuclear spin which can be measured by comparing the PNC effect on different hyperfine components of a transition.

Unfortunately, the weak interaction matrix element is not as large as one might expect from the regular Z^3 enhancement. [2] The reason is that the dominant electronic configurations of the nearly degenerate levels are not mixed by the weak interaction and the PNC effect arises solely from configuration mixing and core polarization. We have previously reported [3] a statistically limited value for the weak interaction matrix element $|H_w| = |2.3 \pm 2.9(statistical) \pm .7(systematic)|$ Hz. This result differs from a theoretical value of $H_w = 70(40)$ Hz obtained using a multi-configuration Hartree-Fock-Dirac calculation. [4] In order to achieve a sensitivity to the weak interaction parameters comparable to the recent measurement in Cs, [5] it will be necessary to measure the PNC effect on different isotopes and hyperfine components to $\sim .1$ %. A weak interaction matrix element smaller than 1 Hz would make these comparisons difficult. With moderate improvements in the the existing apparatus, a new search is now underway with a projected statistical sensitivity to H_w of ~ 10 mHz.

In this paper, we first give a brief description of the PNC-Stark interference technique employed, discuss the previous experimental search, and finally present details of the new search now underway including the results from various spectroscopic measurements.

2 PNC-Stark Interference in Dy

Before we begin this discussion, let us say a few words about the spectroscopic properties of the nearly degenerate pair of levels in Dy which were investigated in an earlier work. [6] The lifetime of the even parity level (designated as A) is 7.9(2) μs. The odd parity level (designated as B) is much longer-lived, with a lifetime > 200 μs. Dysprosium has both even and odd nucleon number stable isotopes (A$= 156 - 164$). The $F = 10.5$ hyperfine components of ^{163}Dy are the closest pair of opposite parity levels, with a separation of only 3.1 MHz. These are the levels selected for the PNC search. These particular hyperfine components are connected by the nuclear spin-independent part of the weak interaction, while the nuclear spin-dependent contribution to the PNC amplitude is highly suppressed. [3]

One advantage of having two closely lying opposite parity levels is that a small external B-field can bring the sublevels (e.g. $|F\ m_F\rangle = |10.5\ 10.5\rangle$) of A and B to near-crossing (Fig. 2). The Hamiltonian of the system can now be

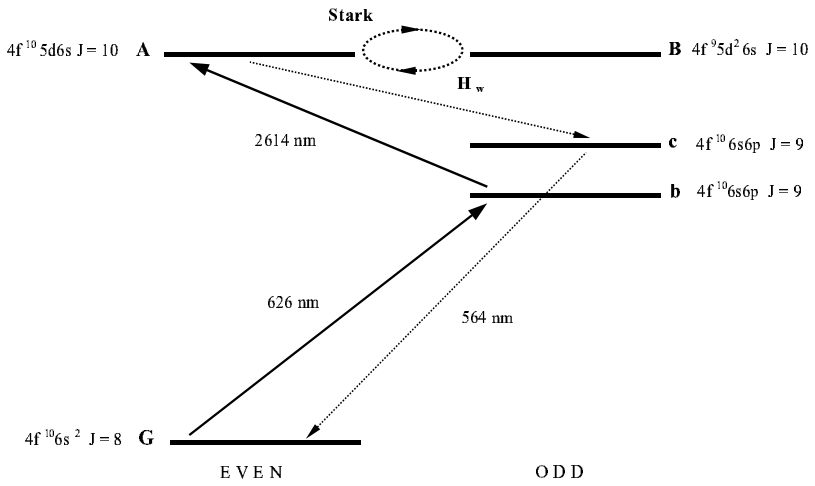

Figure 1: Partial energy level diagram showing PNC and Stark mixing of levels A and B. Solid arrows indicate excitation; dashed arrows indicate fluorescence.

simplified to that of a two-level system:

$$H = \begin{pmatrix} -i\Gamma_{\rm A}/2 & dE + iH_w \\ dE - iH_w & \Delta - i\Gamma_{\rm B}/2 \end{pmatrix}. \tag{1}$$

Here $\Gamma_{\rm A}/2\pi \sim 20$ kHz is the natural width of A; in principle, $\Gamma_{\rm B}/2\pi$ is also the natural width of B, however, because the lifetime of B is much longer than the transit time $T_{\rm B}$ ($\sim$200 μs) of atoms through the E- and B- field region in this particular experiment, $\Gamma_{\rm B}/2\pi \sim 1/2\pi T_B \sim .80$ kHz; Δ is the residual energy separation (decrossing) which depends on the applied magnetic field; iH_w is the PNC matrix element (pure imaginary due to T-reversal invariance); E is the applied electric field; and d is the electric dipole matrix element connecting the sublevels. The magnitude of this matrix element was experimentally determined to be: $|d/2\pi| = 3.8(2)$ kHz/(V/cm).[6] Since dE is real and iH_w is imaginary, interference between these two terms will only occur if E is time-varying with a frequency sufficiently high such that changes in the system are non-adiabatic. This interference can be observed in the temporal dynamics of quantum beats between the two levels. A PNC detection scheme involving rapidly varying E-field was originally proposed for experiments using the $2s - 2p$ levels in hydrogen,[7] but was found to be impractical because of the

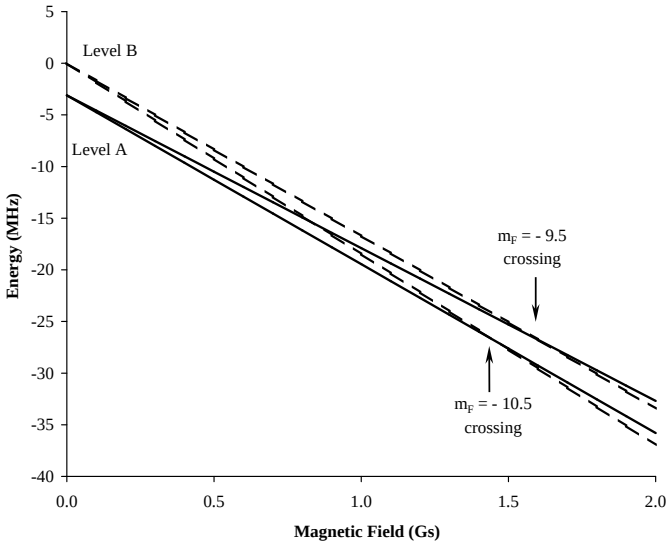

Figure 2: Partial Zeeman structure of ^{163}Dy $F = 10.5$ sublevels of A and B. Zero energy is chosen arbitrarily.

short lifetime of the 2p state. [8]

An approximate solution to the Schrödinger Equation for the two-level system can be obtained using first order time-dependent perturbation theory. In the interaction picture the solution has the form

$$|\psi(t)\rangle = c_{\rm A}(t)|{\rm A}\rangle {\rm e}^{-\Gamma_{\rm A} t/2} + {\rm c_B(t)}|{\rm B}\rangle {\rm e}^{-{\rm i}\Delta {\rm t}} {\rm e}^{-\Gamma_{\rm B} t/2}, \tag{2}$$

(in units where $\hbar = 1$) which leads to two differential equations for $c_{\rm A}(t)$ and $c_{\rm B}(t)$:

$$\dot{c}_{\rm A}(t) = -ic_{\rm B}(t)(dE + iH_w)e^{-i\Omega t}, \tag{3}$$
$$\dot{c}_{\rm B}(t) = -ic_{\rm A}(t)(dE - iH_w)e^{+i\Omega t}, \tag{4}$$

where $\Omega = \Delta + i(\Gamma_{\rm A} - \Gamma_{\rm B})/2$. Let $E = E_0 \cos\omega t$ and let all atoms be in state B at $t = 0$. Since $dE_0 << \omega$ ($\omega/2\pi = 100kHz$) in this experiment, $c_{\rm B}(t)$ is approximately constant in the time-scale of the electric field oscillation; this allows simple integration of Eq. 3 (first order perturbation theory). Making the further approximation $\omega >> |\Omega|$ (again as in the experiment) and only

keeping terms of order dE_0/ω and H_w/Ω, we arrive at

$$\langle \mathrm{A}|\psi(\mathrm{t})\rangle = \frac{-\mathrm{idE_0}}{\omega}\mathrm{e}^{-\mathrm{i}\Delta\mathrm{t}}\mathrm{e}^{-\Gamma_\mathrm{B}\mathrm{t}/2}\sin\omega\mathrm{t} + \mathrm{iH_w}\left[\frac{\mathrm{e}^{-\mathrm{i}\Delta\mathrm{t}}\mathrm{e}^{-\Gamma_\mathrm{B}\mathrm{t}/2} - \mathrm{e}^{-\Gamma_\mathrm{A}\mathrm{t}/2}}{\Omega}\right]. \quad (5)$$

Note that since the Stark and PNC perturbations are off-diagonal (see Eq. 1), the contribution from second order perturbation theory is zero. Returning to Eq. 5, let us consider times t such that $\tau_\mathrm{A} << t < \tau_\mathrm{B}$. This allows further approximations, namely $e^{-\Gamma_\mathrm{B}t/2} \approx 1$ and $e^{-\Gamma_\mathrm{A}t/2} \approx 0$. Thus the population of A is given by

$$|\langle \mathrm{A}|\psi(\mathrm{t})\rangle|^2 = \left(\frac{\mathrm{dE_0}}{\omega}\right)^2 \sin^2\omega\mathrm{t} - \frac{2\mathrm{dE_0H_w}}{\omega}\left(\frac{\Delta}{\Delta^2 + \Gamma_\mathrm{A}^2/4}\right)\sin\omega\mathrm{t}. \quad (6)$$

The first term shows the quantum beat signal due to Stark mixing at the second harmonic of the electric field frequency. The second term shows interference between H_w and dE_0 at the first harmonic. It changes sign with decrossing (see Fig. 3), the overall sign of electric field and magnetic field (the latter reverses the sign of m_F, and correspondingly, that of d). It has the signature of the P-odd, T-even rotational invariant

$$\dot{\boldsymbol{E}} \cdot (\boldsymbol{B} - \boldsymbol{B_c}), \quad (7)$$

where B_c is the magnetic field required to cross the two sublevels (Fig. 2). The magnitude of this term is maximal for $|\Delta| = \Gamma_\mathrm{A}/2$.

A dc electric field, E_{dc}, along the direction of B also contributes an interference term with a first harmonic dependence. Such a field can easily be included in Eq. 3 and contributes a term to the population of A (see Eq. 6) of the form:

$$\frac{2d^2E_0E_{dc}}{\omega}\left(\frac{\Gamma_\mathrm{A}/2}{\Delta^2 + \Gamma_\mathrm{A}^2/4}\right)\sin\omega t. \quad (8)$$

The amplitude of this interference term has a different signature than PNC since it is even with respect to decrossing (Fig. 3).

An estimate of the ratio of PNC-Stark interference term to the leading Stark term can be found using Eq. 6. For $\Delta = \Gamma_\mathrm{A}/2$, this ratio (denoted as ξ) is

$$\xi = \frac{2\omega H_w}{dE_0\Gamma_\mathrm{A}}. \quad (9)$$

In the shot-noise limit, the signal-to-noise ratio S/N is $\xi\sqrt{\dot{N}T}$, where T is the integration time and $\dot{N}$ is the rate of detected fluorescence photons due to

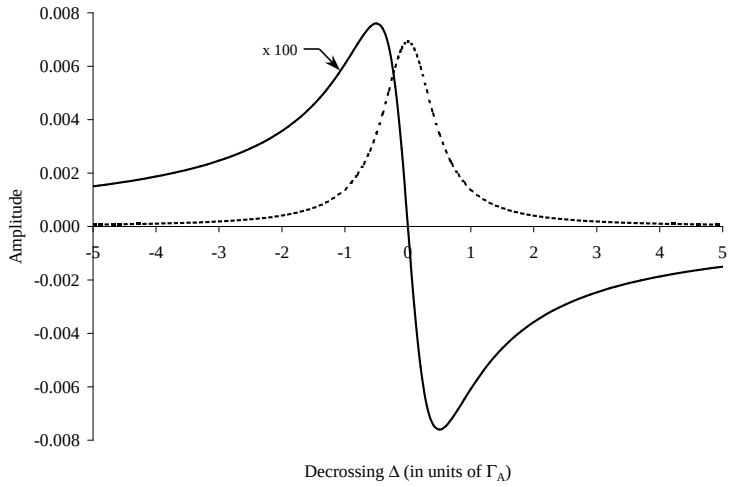

Figure 3: The solid curve shows the calculated PNC-Stark interference term amplitude versus decrossing Δ for $H_w = 5$ Hz (see Eq. 6). For display purposes, this curve has been magnified 100 times. The dashed curve shows the calculated interference term amplitude due to a dc E-field (60 mV/cm)(see Eq. 8). The amplitude of the oscillating E-field is $E_0 = 4$ V/cm.

atoms decaying from state A:

$$\dot{N}T \sim \dot{N}_0 T \left(\frac{d^2 {E_0}^2}{\omega^2} \right) \frac{\Gamma_{\rm A}}{\Gamma_{\rm B}} \leq \dot{N}_0 T. \tag{10}$$

Here $\dot{N}_0$ is the population rate of B. Thus,

$$S/N = \frac{2H_w}{\sqrt{\Gamma_{\rm A}\Gamma_{\rm B}}} \sqrt{\dot{N}_0 T}. \tag{11}$$

Recall that, in this experiment, the lifetime of B is long and, thus, the transit time $T_{\rm B}$ of the atoms through the interaction and detection region is what determines $\Gamma_{\rm B}$. Note that the expression for the ultimate S/N (Eq. 11) does not depend on dE_0 or ω. Furthermore, because we are able to set the decrossing Δ to its optimum value, it is also independent of the initial level separation - a situation radically different from that in traditional PNC experiments. It is also interesting to note that this expression is rather general. For example, a similar result is obtained for an optimized PNC experiment involving $1s \rightarrow 2s$ transitions in hydrogenic systems. [9]

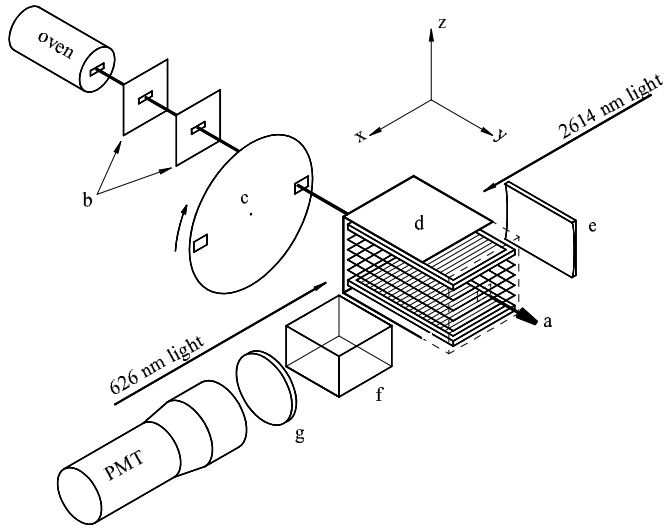

Figure 4: Schematic view of the apparatus (not to scale): (a) atomic beam; (b) collimators; (c) atomic beam chopper; (d) interaction region of atoms with E- and B- fields, with the entire region enclosed in a magnetic shield (not shown), (e) mirror (other mirrors are installed above and below the E-field wire grids); (f) light pipe; (g) interference filter; PMT: photomultiplier tube.

3 Previous Experimental Search

We will now give an overview of the previous search. A more detailed description can be found in Ref. [3].

3.1 Experimental overview

Fig. 4 shows a schematic view of the apparatus. An atomic beam of Dy was produced by an effusive oven source at $T = 1500$ K. After passing through collimators, the atomic beam encountered a chopper wheel which was used to block oven blackbody radiation. This wheel triggered the subsequent laser pulses, E- and B- fields, and detection electronics. The atomic beam then entered the interaction region where the atoms are first populated. The volume of the interaction region was $\sim (3 \times 5 \times 10)$ cm^3. State A was initially populated by two-step excitation from the ground state using consecutive laser pulses at 626 and 2614 nm, respectively (Fig. 1). Each pulse had an energy ~ 3 mJ and a duration of ~ 7 ns. The pulse repetition rate was 10 Hz.

A B-field was applied to bring the sublevels with $|m_F| = 10.5$ of A and B nearly to crossing. This field was produced by eight turns of gold plated copper wire surrounding the interaction region. High homogeneity was achieved by providing a yoke for the return of magnetic flux lines. This yoke was made of high-permeability magnetic material. The fractional inhomogeneity in the magnitude of the B-field was measured to be $\leq 10^{-3}$ over most of the volume of the interaction region.

After state A was populated, an E-field sequence was applied. An initial square π pulse transferred atoms from state A ($|m_F| = 10.5$) to the much longer-lived state B ($|m_F| = 10.5$). A time delay of ≈ 70 μs allowed atoms to move into the field of view of the light detection system and also gave atoms remaining in state A sufficient time to decay. Finally, the sinusoidal E-field which provided the Stark mixing was applied. For shot noise to be comparable to electronic noise, an amplitude of $\sim$ 4 V/cm was chosen. The E-field was formed between two wire grids. Wire grids were used in order to minimize surface area and thus stray charge accumulation. They were constructed by winding 50-μm diam Be-Cu wire around brass frames. In order to achieve a high level of E-field homogeneity near the grid fringes, four additional wires were wrapped adjacent to the magnetic field wires. A resisitive voltage divider distributed the potential among these wires. Using computer modeling, an optimum resistor configuration was found, which produced a calculated fractional inhomogeneity of $\leq 5 \times 10^{-4}$ over most of the volume of the interaction region. Note, we only needed to consider z components of the E- and B-fields. Although other components would tend to mix in a contribution from the $|m_F| = 9.5$ sublevel, this contribution is negligible due to the large energy separation ($\sim$ 300 kHz) and the smaller dipole matrix element connecting it to the $|m_F| = 10.5$ sublevel.

Mirrors surrounding the E- and B- field interaction region directed fluorescence towards a lucite light pipe and onto a photomultiplier tube. Time resolved quantum beats of state A were observed by monitoring 564-nm light from the second step of decay fluorescence (Fig. 1).

3.2 Data and results

Fig. 5 shows a typical data curve with the sinusoidal E-field superimposed for the purpose of display. The data curve corresponds to an average of 200 laser shots ($\sim$ 20 s of real time). A value for H_w is found by fitting a function to this data curve. This function takes into account the fluorescence lineshape, backgrounds, and light detection efficiency. One data file consists of four such curves, or channels, corresponding to the four combinations of the signs of E-

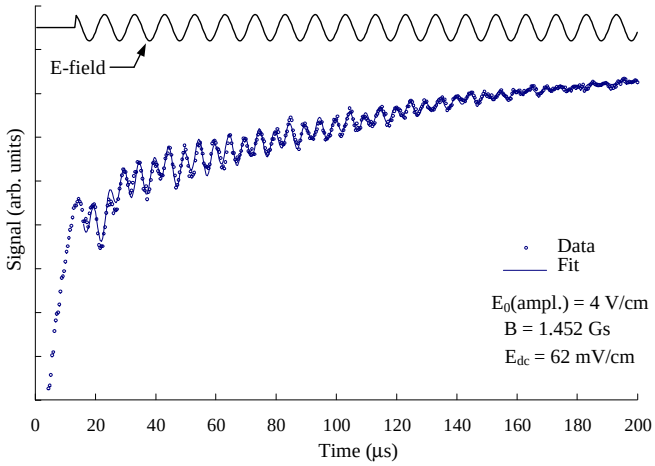

Figure 5: Typical data from a given channel. Best-fit value for E_{dc} has been used for the shown fit. The first-harmonic term due to E_{dc} can readily be seen. The data curve corresponds to an average of 200 laser shots (total real time $\sim$ 20 s). Also the cosine E-field has been superimposed for the purpose of display.

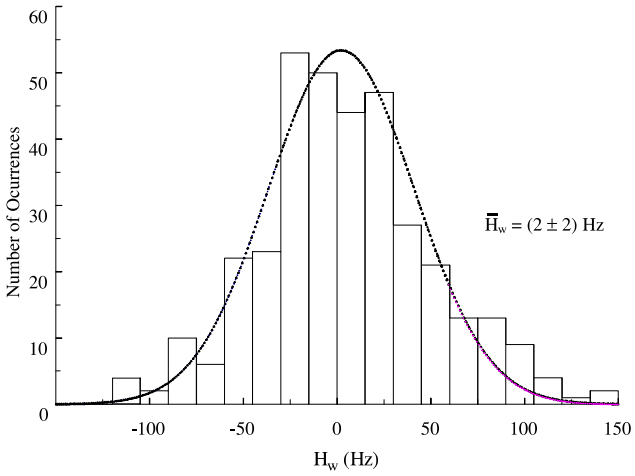

Figure 6: Histogram of all values of fitted H_w from each individual channel. The dashed curve is a best-fit Gaussian.

and B- fields. Files were taken above ($\Delta \simeq \Gamma_A/2$), below ($\Delta \simeq -\Gamma_A/2$), and on ($\Delta \simeq 0$) crossing.

More than thirty hours of data were taken. Figure 6 shows a histogram of fitted H_w from all channels along with a best-fit Gaussian. Table 1 shows the same fitted values of H_w grouped according to channels and according to decrossing Δ. No statistically significant discrepancies are observed. The final value for $|H_w|$ is $|2.3 \pm 2.9(statistical) \pm .7(systematic)|$ Hz. The sign of the central value of H_w is the same as that of the electric-dipole matrix element d. A cancellation between the nuclear-spin-dependent (NSD) and spin-independent contributions is unlikely because $F = 10.5$ hyperfine components are particularly insensitive to NSD effects.[3]

The value for systematic error was estimated by considering various imperfections which can mimic a PNC effect. These imperfections include various combinations of E- and B- field gradients, residual stray fields, etc.

Table 1: Fitted values for H_w grouped according to channels and to decrossing Δ.

	Ch. 1 (E_+B_+)	Ch. 2 (E_-B_+)	Ch. 3 (E_+B_-)	Ch. 4 (E_-B_-)
H_w (Hz)	$-.9 \pm 5.6$	-1.0 ± 5.7	$.5 \pm 5.5$	10.9 ± 5.6

	$\Delta < 0$	$\Delta > 0$
H_w (Hz)	$.1 \pm 3.5$	9.4 ± 4.9

4 New Experimental Search

With a maximum pulse laser repetition rate of 10 Hz, the duty cycle of the previous experiment was limited to 10^{-4}. A cw scheme of PNC detection would achieve a 100 % duty cycle. With a comparable integration time as in the previous search, this increased counting rate would, in principle, allow a statistical sensitivity to H_w of $\sim$ 10 mHz. Such a scheme is the basis for a new search currently underway. A new population scheme will be used which involves two-laser excitation to a high-lying even parity state followed by a transition to state B. Single-mode diode lasers are commercially available for all three transitions. Also, in order to excite the full transverse Doppler width, an efficient scheme for adiabatic population transfer is considered. Finally, an additional order of magnitude increase in the counting rate can be achieved by optically pre-pumping atoms into one Zeeman sublevel in the ground state prior to the excitation of B.

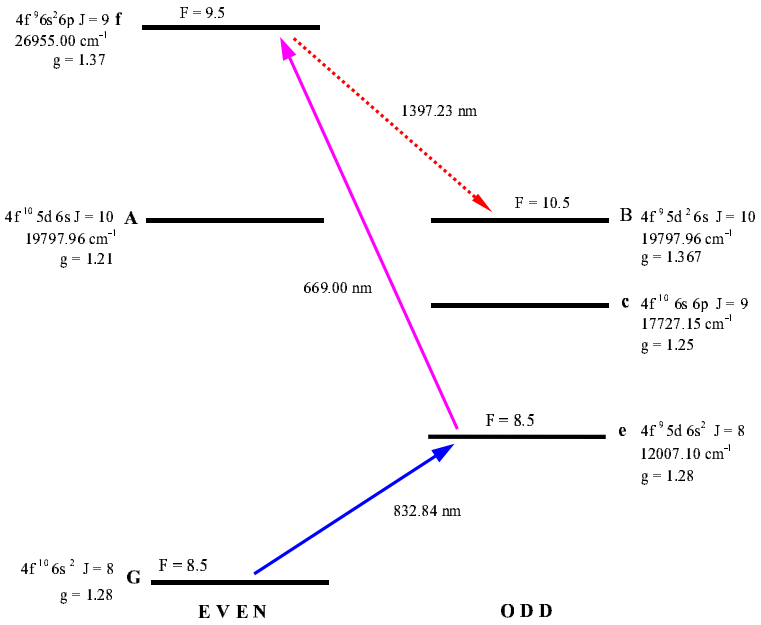

Figure 7: New population scheme. Solid arrows indicate excitation; dashed arrow indicates spontaneous or stimulated decay.

4.1 New population scheme

Figure 7 shows the transitions used in the new cw excitation scheme. The G $\rightarrow$ e transition is at 833 nm. The next transition occurs at 669 nm and excites the atom to state f. The final transition is to the odd parity state B at 1397 nm. In contrast to the previous population scheme, a π pulse of E-field (see Sect. 3.1) is unnecessary since B is directly populated. In order to populate the $F = 10.5$ component of state B and since $\Delta F = \Delta J$ transitions are the strongest, [10] the hyperfine levels of interest for states G, e, and f are F =8.5, 8.5, and 9.5, respectively.

Using pulsed lasers and time-resolved fluorescence detection, the lifetimes of e and f have been measured to be $16.5 \pm 2.6\ \mu s$ and $432 \pm 5\ ns$, respectively. These measurements were carried out in a manner similar to our earlier work on lifetimes in Dy, [6] Yb, [11] and Sm. [12]

The hyperfine structure and isotope shifts of the G $\rightarrow$ e transition (Fig. 8) were measured by detecting absorption of an external-cavity single-frequency

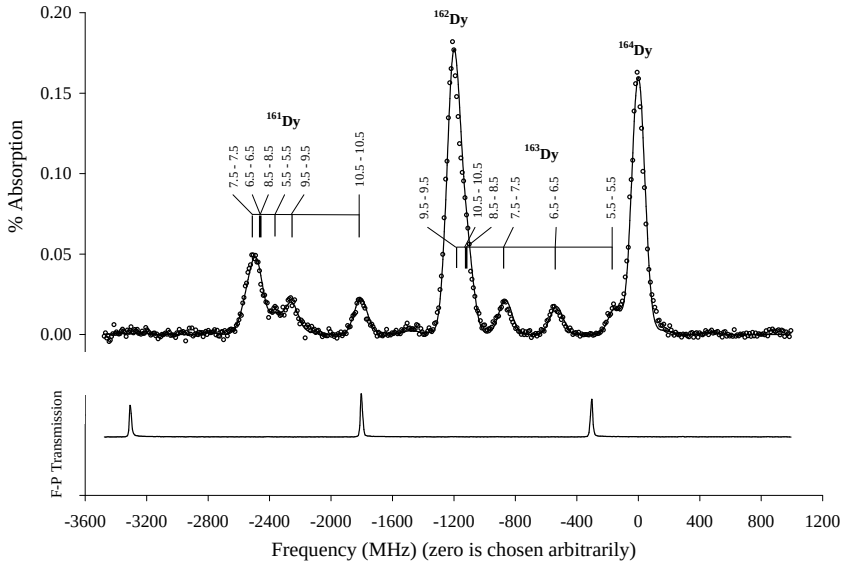

Figure 8: Hyperfine structure and isotope shifts of the G $\rightarrow$ e transition. Solid line represents best-fit curve. Only the strongest hyperfine lines have been identified. A transmission curve from a Fabry-Perot interferometer (FSR= 1.50 GHz) has been superimposed to provide frequency markers.

diode laser. The measured hyperfine constants and the isotope shift energies agree well with an earlier result.[13] The hyperfine structure and isotope shifts of the e $\rightarrow$ f transition have yet to be measured.

The relevant decays of f are shown in Fig. 9. Assuming only spontaneous decays from state f, the f $\rightarrow$ B branching ratio determines the population efficiency of state B. We have measured this branching ratio using pulsed lasers and have found it to be .30 $\pm$ .09. Thus, for the time being, the introduction of a third laser is not needed. We will now briefly describe the details of this measurement and also present results for other decays from state f.

Figure 10 shows an exploded view of the laser- atomic beam region. State f was populated by two-step excitation using consecutive laser pulses at 741 and 743 nm, respectively. A germanium photodiode (EG&G Judson J16) was used to detect infrared decay channels (1.18-1.94 μm). These signals were compared to visible channels detected by a red-sensitive photomultiplier tube (Philips XP2203B). The detectors were placed, one at a time, into a holder which extended into the vacuum chamber. Comparing infrared to visible sig-

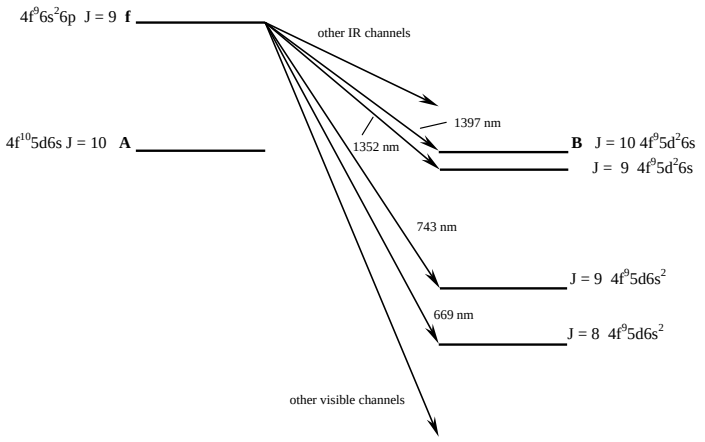

Figure 9: Decays of state f.

nals involved taking data with one detector, interchanging detectors, and then taking data with the other. The distance from the laser-atomic beam interaction region to the detector was ≈ 3.4 cm. To increase light collection, a spherical mirror ($f = 2.1$ cm) was placed ≈ 3.3 cm from the laser-atomic beam interaction region. It roughly focused fluorescence onto the detector. Color glass and/or narrow-band interference filters selected desired wavelengths. To accurately account for the different light collection geometries of the two detectors as well as interference filter dependences upon different incidence angles, a Monte Carlo simulation was performed. Signals were compared to the 669 nm signal because it was large (due to the high PMT sensitivity at this wavelength) and free of background signals. The 743 nm signal was comparable in size but possessed a large background due to the relatively close second-step of fluorescence to the ground state G at 741 nm. In order to make accurate comparisons of the infrared to visible signals, it is necessary to know well the response of each detector. For the PMT, using various laser sources, the product of gain and quantum efficiency at several wavelengths was determined relative to a calibrated power meter. These results were consistent with a single value provided by the manufacturer's test data sheets. For the Ge photodiode, only one laser at 833 nm was used to determine the responsivity. Typical responsivity data, found in the detector catalog, was then scaled to this measured value.

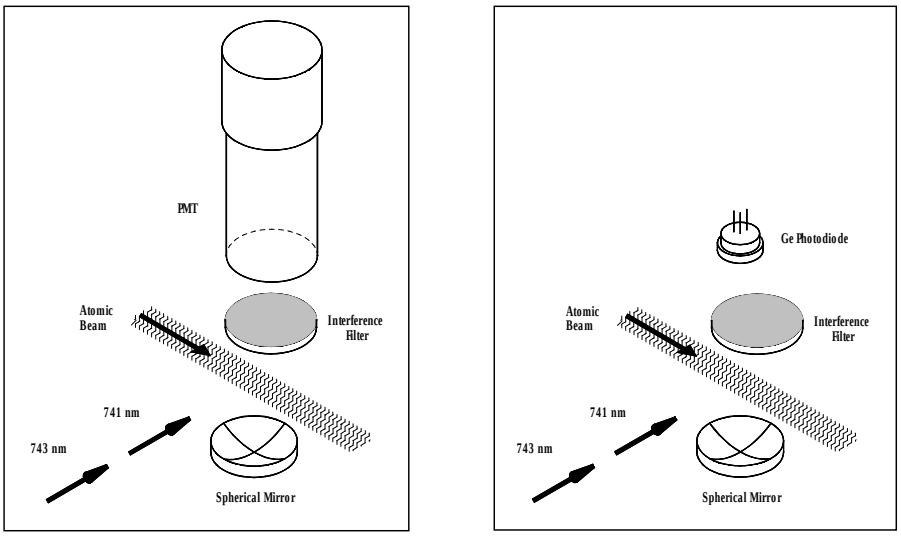

Figure 10: Exploded view of the laser-atomic beam interaction region used in the branching ratio and lifetime measurements, (a) with the PMT to detect visible signals. Note: the interference filter and PMT are not centered on the intersection of the laser and atomic beam because of technical reasons; (b) with the germanium photodiode to detect infrared signals.

Table 2: Branching ratios of state f.

Transition	Branching Ratio
1397 nm ($\rightarrow B$)	$.30 \pm .09$
1352 nm	$.33 \pm .10$
other IR channels	$\leq .37$
743 nm	$.05 \pm .01$
669 nm ($\rightarrow e$)	$.017 \pm .004$
other vis. channels	$< .003$

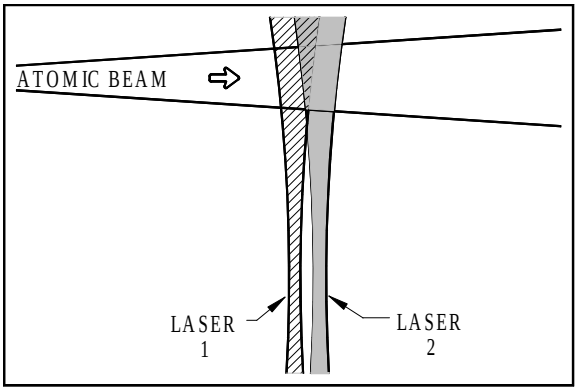

Figure 11: Pictorial representation of atomic beam intersecting two Gaussian laser beams.

Table 2 shows the results which includes the transition of interest (f→B). It is worth noting that the uncertainty of the photodiode responsivity contributes little to the final uncertainty because the infrared transitions are so strong. In fact, the greatest source of uncertainty was due to laser frequency drifts in the time that it takes to exchange detectors.

4.2 Adiabatic passage

In contrast to pulsed lasers, cw lasers normally have a much narrower linewidth. Thus, only a particular transverse velocity group of atoms interacts with light. This can be overcome by broadening the laser linewidth with a frequency modulator (e.g. an acoustic-optic modulator). A more elegant solution relies upon a coherent population technique[14] analogous to the adiabatic fast passage technique used in nuclear magnetic resonance. The transverse Doppler width of the weakly collimated ($\sim$ 1:10) atomic beam is $\sim$ 100 MHz. By using cylindrical lenses to produce laser beams with similar divergences (see Fig. 11), one ensures that each velocity group of atoms will encounter chirped light frequencies, sweeping from one side of resonance to the other which leads to adiabatic transfer to state f.

We have modeled this technique for the transitions in dysprosium using partially overlapping laser beams. Both two-laser excitation (at 833 and 669 nm) and spontaneous emission (at 1397 nm), as well as, three-laser excitation (for all three transitions) were considered. The results for these two cases show a robust and nearly complete transfer of atoms in the ground state to

states f and B, respectively, with diode laser powers of a few mW. We are now beginning to experimentally implement this technique.

5 Concluding Remarks

A new search for PNC in dysprosium is now underway. This entails using the same interaction region as in our previous experiment, but a new cw scheme for state population and PNC detection. A few orders of magnitude improvement in statistical sensitivity is expected. This will hopefully unambiguously determine the size of the PNC effect. If the effect turns out to be on the order of the current upper limit, it will allow for tests of the Standard Model as well as observation of nuclear spin dependent PNC effects, particularly, the nuclear anapole moment).

Acknowledgments

We would like to thank D. Weiss for drawing our attention to the use of diverging laser beams. This research was supported by NSF Grant No. PHY-9311610 and by the University of California, Berkeley COR Faculty and Junior Faculty Research Grants.

References

1. V.A. Dzuba, V.V. Flambaum, and I.B. Khriplovich, *Z. Phys.* D **1**, 243 (1986).
2. M.A. Bouchiat and C. Bouchiat, *J. Phys.* **35**, 899 (1974).
3. A.-T. Nguyen, D. Budker, D. DeMille, and M. Zolotorev, *Phys. Rev.* A **56**, 3453 (1997).
4. V.A. Dzuba, V.V. Flambaum, and M.G. Kozlov, *Phys. Rev.* A **50**, 3812 (1994).
5. C.S. Wood et. al., Science **275**, 1759 (1997).
6. D. Budker, D. DeMille, E.D. Commins, and M. Zolotorev, *Phys. Rev.* A **50**, 132 (1994).
7. R.R. Lewis and W.L. Williams, *Phys. Lett.* B **59**, 70 (1975).
8. R.W. Dunford, Ph.D. dissertation, Univ. of Michigan, 1978 (unpublished), available from University Microfilms in Ann Arbor, MI.
9. M. Zolotorev and D. Budker, *Phys. Rev. Lett.* **78**, 25 (1997); see also elsewhere in these proceedings.
10. I.I. Sobelman, *Atomic Spectra and Radiative Transitions* (Springer-Verlag, New York, 1992), p. 211.
11. C.J. Bowers et. al., *Phys. Rev.* A **53**, 3103 (1996).

12. S. Rochester, D. Budker, D. DeMille, and M. Zolotorev, Lawrence Berkeley National Laboratory Preprint No. 42227, submitted for publication.
13. R.J. Lipert, S.C. Lee, *Appl. Phys.* B **57**, 373 (1993) (Note a misprint: values for the hyperfine constants of ^{163}Dy and ^{161}Dy in Table 3 are switched.
14. C.R. Ekstrom, et. al., Optics Comm. **123**, 505 (1996).